

**Periodic variations in the local surface potential of Si(111)-(5×2)-Au**S. Polei,<sup>1,\*</sup> I. Barke,<sup>1</sup> S. C. Erwin,<sup>2</sup> and K-H. Meiwes-Broer<sup>1</sup><sup>1</sup>*Department of Physics, University of Rostock, D-18051 Rostock, Germany*<sup>2</sup>*Center for Computational Materials Science, Naval Research Laboratory, Washington, D.C. 20375, USA*

(Received 2 November 2011; revised manuscript received 9 March 2012; published 6 April 2012)

The image-state-derived field-emission resonances (FERs) on a Si(111)-(7 × 7) surface that is partially covered by the gold-induced Si(111)-(5 × 2)-Au reconstruction, were probed by scanning tunneling spectroscopy measurements. On Si(111)-(5 × 2)-Au, a shift of the FER peak positions is observed compared to the bare 7 × 7 surface. Spatially resolved  $dI/dV$  maps reveal a periodic variation of the higher-order FERs in the direction perpendicular to the chains of the quasi-one-dimensional Si(111)-(5 × 2)-Au reconstruction. The effect appears on a length scale of less than one nanometer and can be attributed to the local surface potential. Simple one-dimensional models reproduce the first seven FERs perfectly and allow extraction of the potential landscape. This landscape is confirmed by density-functional theory calculations, revealing an attractive well above the graphitic Si honeycomb chains due to low electron density.

DOI: [10.1103/PhysRevB.85.165414](https://doi.org/10.1103/PhysRevB.85.165414)

PACS number(s): 73.22.-f, 68.37.Ef, 71.15.Mb, 73.20.-r

**I. INTRODUCTION**

Gold-induced atomic chains on flat and vicinal semiconductor surfaces have gained considerable interest in recent years because they are a promising model system for low-dimensional physics that is accessible by both experimental and theoretical methods. On flat Si(111), a chain system exists for 0.6 monolayer (ML) gold coverage, where one ML is referenced to the number of silicon atoms in a surface layer. The atomic structure of this Si(111)-(5 × 2)-Au reconstruction (in the following referred to as 5 × 2) has been solved recently using a combination of precise coverage determination,<sup>1</sup> high-resolution scanning tunneling microscopy (STM), angle-resolved photoelectron spectroscopy (ARPES), and density-functional theory (DFT) calculations.<sup>2</sup>

In this work, the local surface potential (LSP) above the 5 × 2 surface is investigated in real space. On nanostructured surfaces, the LSP is typically not homogeneous, which results in lateral components of the electric field. It has been shown to play an important role for various processes at surfaces, including Rashba spin-orbit splitting,<sup>3</sup> as well as catalytic<sup>4</sup> and adsorbate<sup>5</sup> behavior, and it contributes to the local work function (LWF),<sup>4</sup> which is one of the most fundamental physical properties of a nonuniform surface. Scanning tunneling spectroscopy (STS) is used to probe the LSP with high spatial resolution. The STM is operated in a field-emission mode at large positive sample voltage, where tunneling is enhanced by image-potential states that are modified by the electric field between the tip and sample. These confined states appear as so-called field-emission resonances (FERs) or Gundlach oscillations in STS curves.<sup>6–8</sup> They are related to image-potential states, which have been intensely studied on metal and dielectric surfaces,<sup>8–10</sup> and were proposed to be used as scalable quantum bits.<sup>11</sup> Quasi-one-dimensional surfaces related to the present system have been examined in reciprocal space by two-photon photoemission<sup>12–17</sup> and inverse photoemission,<sup>18–20</sup> but investigations in real space are rare. In STS curves, the energy position of the FER at the location of the tip is a measure for the LSP, which can be obtained by fitting the solution of the one-dimensional Schrödinger equation in the direction perpendicular to the

surface.<sup>5,21,22</sup> Realistic potential models include the contact potential, the image potential, and the tip-sample potential induced by the tunneling voltage. As shown in this work, the periodic potential variations that decrease as a function of the distance to the sample require an extended model that includes a Laplace-derived modulation decay.

The structure of the paper is as follows: The starting point is the comparison of spatially averaged FER spectra on Si(111)-(7 × 7) versus Si(111)-(5 × 2)-Au. Then, on 5 × 2, periodic modulations of the LSP on the atomic scale are investigated in detail by STS and DFT. It is shown that a modification of the one-dimensional potential model is necessary since the tip-surface distance is of a similar dimension to the lateral period length. Finally, the mechanism for asymmetrically suppressed FER peaks observed in STS curves is explained by simple numerical simulations that account for the varying tip-surface distance during spectroscopy.

**II. METHODS**

The Si(111) substrate was degassed at 650 °C for one hour, followed by repeated flashing to 1250 °C, resulting in an atomically clean Si(111)-(7 × 7) surface (in the following referred to as 7 × 7). In order to partially cover the substrate with 5 × 2, less than 0.6 monolayers of Au were evaporated at 650 °C. The patch size can be tuned by the temperature of a postanneal. For this work, 850 °C was used, resulting in several-hundred-nm-large and well-defined patches of Si(111)-(5 × 2)-Au. The base pressure for sample preparation and subsequent STM investigations was less than 10<sup>-10</sup> mbar. The experiments were performed in a commercial low-temperature STM operated at 78 K. The differential conductivity curves  $dI/dV$  were obtained by a lock-in technique in a closed-loop mode with a setpoint of 0.1 nA. Frequencies between 5 and 9 kHz and modulation voltages between 20 and 50 mV<sub>rms</sub> were used, resulting in an energy resolution of the order of 100 mV. The corresponding tip displacement  $z(V)$  was recorded simultaneously. For all measurements, a single W tip was used prepared by standard electrochemical etching followed by in-vacuo heating and Ar self-sputtering.<sup>23</sup>

First-principles electronic-structure calculations were used to determine the equilibrium geometry of Si(111)-(5 × 2)-Au and the self-consistent electrostatic potential near the surface. The structural model was the same as that proposed in Ref. 2. The calculations were performed in a slab geometry with four layers of Si plus the reconstructed top surface layer and a vacuum region of 15 Å. All atomic positions were relaxed, except the bottom Si layer and its passivating hydrogen layer, until the largest force component on every atom was below 0.01 eV/Å. Total energies and forces were calculated within the Perdew-Burke-Ernzerhof (PBE) generalized-gradient approximation to DFT using projector-augmented-wave potentials, as implemented in VASP.<sup>24,25</sup> The plane-wave cutoff was 250 eV, and a 2 × 2 grid was used to sample the surface Brillouin zone.

### III. RESULTS AND DISCUSSION

#### A. Comparison between 5 × 2 and 7 × 7

In the STM topography image of a 5 × 2 patch [Fig. 1(a)], two alternating elements of the chain structure can be distinguished: gold-silicide chains (AuSi), which appear as bright stripes, and dark silicon honeycomb chains (Si-HC). Additional Si adatoms appear as bright protrusions. In Fig. 1(b), the structural model based on first-principles total-energy calculations<sup>2</sup> is shown. The chains reveal a periodicity of 1.67 nm in the perpendicular direction and are found to extend up to some μm in length, depending on the patch size.

In a first step, the 5 × 2 chain structure is compared to the pristine 7 × 7 surface. In Fig. 2(a), a topography image of the 7 × 7 surface together with a typical 5 × 2 patch is shown. Corresponding  $dI/dV$  spectra averaged over a 7 × 7 and 5 × 2 patch are shown in Figs. 2(b) and 2(c). For large positive voltages (i.e., >4 V), pronounced peaks are observed.

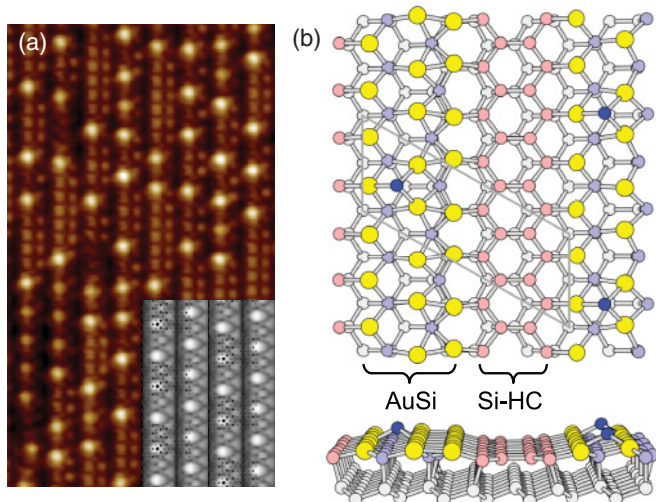


FIG. 1. (Color online) (a) Topography (15 × 26 nm,  $U_T = +0.8$  V,  $I_T = 30$  pA) of the Si(111)-(5 × 2)-Au reconstruction. Chains of AuSi appear bright and chains of Si-HC appear dark. (b) Structural model of the (5 × 2)-Au reconstruction as obtained from first-principles total-energy calculations (Ref. 2). Inset of (a): Simulated STM topography based on structural model shown in (b) (Ref. 2).

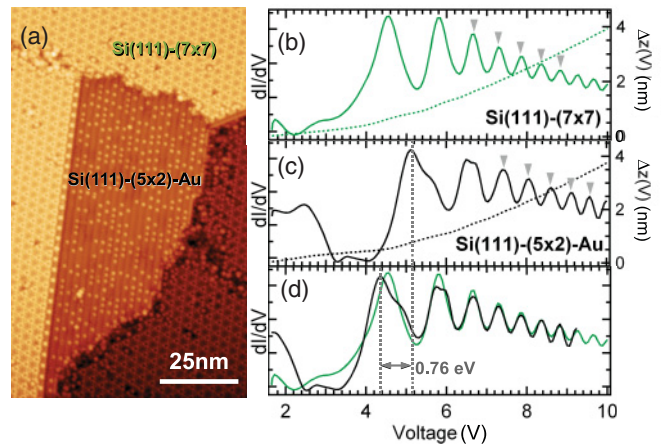


FIG. 2. (Color online) (a) STM image of the 7 × 7 surface and a 5 × 2 patch. (b) Averaged  $dI/dV$  spectra (solid line) and tip displacement  $z(V)$  (dashed line) on 7 × 7 and (c) 5 × 2, respectively. (d) The peak positions of the 5 × 2 spectrum shifted horizontally by 0.76 eV match those of the 7 × 7 curve, indicating an overall work-function difference.

As seen in Figs. 2(b) and 2(c), the spatially averaged FERs on 7 × 7 areas start to appear at voltages of 4–5 V, in contrast to 5–6 V on patches of 5 × 2. Such differences in the voltage onset of the FER series directly reflect LWF variations.<sup>21,26</sup> In fact, the entire  $dI/dV$  curves in Figs. 2(b) and 2(c) can be brought into accordance simply by a horizontal offset  $\Delta E$ , as shown in Fig. 2(d). The best agreement is achieved for  $\Delta E = -0.76$  eV. While the higher-order FER peak positions coincide perfectly, small deviations are visible for the first state caused by a fine structure (shoulder) in the 5 × 2 curve, which is discussed in Sec. III C.

A constant shift of all spectral features is only possible if the LWF for both structures is different by  $\Delta E$  and all other contributions to the FER energies remain constant. The same result is obtained using a simple one-dimensional model: for higher-order FERs, the potential can be assumed to be infinite inside the bulk and linearly increasing in the direction of the tip (i.e., triangular shape).<sup>27</sup> The energy eigenvalues are then

$$V_n = \phi + \left(\frac{3\pi}{2\sqrt{2}}\right)^{\frac{2}{3}} \left(\frac{e^2 F^2 \hbar^2}{m_e}\right)^{\frac{1}{3}} \left(n - \frac{1}{4}\right)^{\frac{2}{3}}, \quad (1)$$

where  $e$  is the elementary charge,  $F$  is the external field,  $m_e$  is the mass of an electron,  $n$  is the consecutive number of the FERs, and  $\phi$  is the LWF. A fit to the experimental data with  $F$  and  $\phi$  as free parameters results in the FER positions indicated by arrows in Figs. 2(b) and 2(c). As the model is only valid for higher-order FERs, the first two states were excluded from the calculations. Despite its simplicity, the model matches the experiment well.<sup>28</sup> The fit yields a LWF difference,  $\Delta\phi = (0.76 \pm 0.05)$  eV.

The total LWF difference comprises two surface-related contributions: first, both structures have significantly different Fermi-level pinning of about  $\Delta E_f = -0.45$  eV.<sup>29,30</sup> The remaining difference is attributed to surface-dipole effects, which now can be estimated to be  $\Delta E_D = 0.31$  eV. This value is comparable to the effect of polar molecules adsorbed on 5 × 2.<sup>31</sup> In addition, the LWF of 5 × 2 can be estimated from

the obtained  $\Delta\phi$  and the LWF of  $7 \times 7$  ( $\approx 4.6$  eV)<sup>32</sup> to  $\approx 5.4$  eV. In earlier ultraviolet photoelectron spectroscopy studies,  $\Delta\phi = 0.34$  eV has been reported,<sup>33</sup> while in spatially resolved Kelvin probe measurements,  $\Delta\phi = 0.5$  eV was found.<sup>34</sup> The origin of this experimental spread is left as a subject for future investigations.

### B. Periodic potential variations

The spatially dependent FER spectra of a region containing both  $7 \times 7$  and  $5 \times 2$  are presented in Fig. 3. The  $dI/dV$  map in Fig. 3(b) is obtained by averaging the  $dI/dV(x, y, V)$  data along the  $x$  direction [parallel to the  $5 \times 2$  chains shown in Fig. 3(a)]. Obviously, the LWF difference discussed in the previous section occurs on a length scale of about 1 nm.

In the following, the spectra of the  $5 \times 2$  area are discussed in detail. A pronounced periodic modulation of the  $dI/dV$  signal is found in the direction perpendicular to the chains ( $y$  direction) with a periodicity of  $\approx 1.7$  nm, matching the  $5 \times 2$  interchain distance. A comparison of the  $dI/dV$  map to the topography [dashed lines in Figs. 3(a) and 3(b)] reveals that on the Si-HC chains, the first FER appears at 5.1 eV, while on the AuSi chain, it is located at 5.66 eV. No significant influence of the Si adatoms on the FER positions is observed.

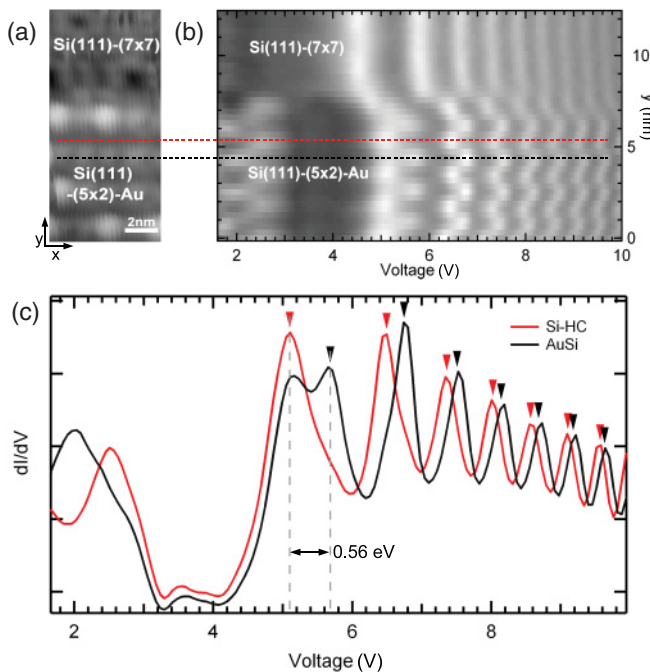


FIG. 3. (Color online) (a) STM topography at a transition between  $7 \times 7$  and  $5 \times 2$ . The chains are oriented in the  $x$  direction. (b)  $dI/dV$  map of the area shown in (a) obtained by averaging a complete  $dI/dV(x, y, V)$  data set along the  $x$  direction (parallel to the  $5 \times 2$  chains). Pronounced peaks found between 4 and 10 V represent FERs. Red and black dashed lines indicate AuSi and Si-HC chains, respectively. (c) Averaged  $dI/dV$  spectra measured over AuSi chains (black line) and Si-HC chains (red line). On the AuSi chains, the FERs are shifted to higher voltages with respect to the FERs on the Si-HC chains. In addition, a distinct splitting of the first FER of the AuSi chains is present. Arrows indicate calculated FER positions matching the observed peak positions perfectly.

For a further analysis,  $dI/dV$  spectra averaged over areas of the AuSi chains are compared to those of the Si-HC chains in Fig. 3(c). Here the FERs appear as peaks in the range of 5 to 10 V. Two main differences are evident: First, the higher-order FERs (starting from  $n = 2$ ) on the AuSi chains are shifted toward higher voltages compared to those of the Si-HC chains, with decreasing differences for higher voltages. Second, the first FER of the AuSi chains shows a pronounced double-peak feature, while it consists of a single peak in the Si-HC chain spectrum. The first peak in the  $n = 1$  AuSi FER is attributed to a remnant of the  $n = 1$  Si-HC FER, whose origin is addressed in detail below. Thus, the energy position of the first FER differs by 0.56 eV, as indicated in the figure. The difference of the LSP can be expected to be of a similar magnitude.<sup>35</sup>

In contrast to the LWF comparison on patches of  $5 \times 2$  and  $7 \times 7$  (constant shift in Fig. 3), the periodicity  $a = 1.7$  nm of the chains is now comparable to the tip-sample distance. Consequently, the surface-potential variations induced by the chains decay in a nonlinear way into the vacuum. Thus the simple assumption of a triangular tunneling barrier as used before for the higher-order FERs is not valid here. Energy shifts of the FERs on a short lateral length scale directly reflect the surface potential.<sup>5</sup> With increasing  $n$ , the energetic positions of the FER states are determined by a larger relevant  $z$ -range of the potential. From Laplace's equation, it follows that the first Fourier component of a periodic potential modulation,  $\Delta\Phi(z = z_0, y) = V_0 \sin(\frac{2\pi}{a}y)$  (with amplitude  $V_0$  and periodicity  $a$ ), at a certain distance  $z_0$  from the surface decays exponentially according to  $\Delta\Phi(z, y) = V_0 \sin(\frac{2\pi}{a}y) \exp[-2\pi/a(z - z_0)]$ .

In order to quantitatively reproduce the measured voltages for all FERs, the time-independent Schrodinger equation was solved numerically for each voltage in the relevant range using the Numerov scheme.<sup>36</sup> The model potential (Fig. 4) includes the exponentially decaying LSP difference (see inset in Fig. 4), the work function of tip and sample ( $\Phi_t$  and  $\Phi_{5 \times 2}$ , respectively) whose difference results in a contact potential, the image potential of the tip and sample including the dielectric constant of the respective material,<sup>37</sup> and the potential induced by the tip-sample voltage.<sup>38</sup> Measured  $z(V)$  curves are used for modeling the geometry of the potential, leaving an unknown constant offset  $d_0$  as a fit parameter. In a simultaneous fit of the model to peak positions of both spectra in Fig. 3(c), the remaining fit parameters are the (spatially averaged) work functions of the tip and sample, the location of the image plane at the sample surface  $z_i$ , and the LSP difference (i.e.,  $2V_0$ ) between AuSi and Si-HC at distance  $z_0$ . Note that  $z_0$  can be chosen arbitrarily without loss of generality. A reasonable choice is the distance corresponding to the expectation value  $\langle z \rangle$  of the first FER wave function because  $V_0$  can then be directly compared to the measured shift of the first FER (see below). The calculated FER positions for the best fit are indicated by arrows in Fig. 3 and perfectly match the measured peak positions with deviations of  $< 20$  meV. The fit results in  $\Phi_{5 \times 2} = 5.52 \pm 0.03$  eV, which is remarkably close to the work function  $\Phi \approx 5.4$  eV obtained from comparison to the  $7 \times 7$  substrate (see discussion in the context of Fig. 2 above). A mean expectation value  $\langle \bar{z} \rangle = (\langle z_{\text{AuSi}} \rangle + \langle z_{\text{Si-HC}} \rangle) / 2 = 3.2$  Å can be derived from the first FER wave function, in agreement with a similar estimation

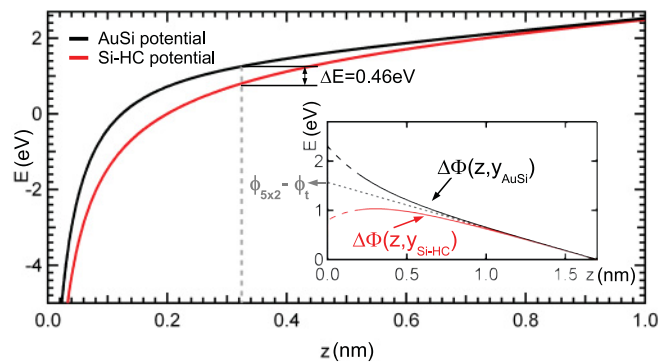


FIG. 4. (Color online) Simple model for the electrostatic potential above AuSi chains (black lines) and Si-HC chains (red lines) for a tip-sample voltage of 5.5 V. Toward the vacuum, the exponential equilibration of the LSP variations is taken into account. The effective potential variation experienced by the electron states of the first FER is 0.46 eV. The resulting FER eigenenergies are indicated by arrows in Fig. 3(c). Inset: components  $[\Delta\Phi(z, y_{\text{AuSi}}), \Delta\Phi(z, y_{\text{Si-HC}})]$  of the potential that are dependent on the  $y$  direction (perpendicular to the chains) including the contact potential due to work-function differences,  $\phi_{5 \times 2} - \phi_t$ , of the sample and tip. At distances of more than  $\approx 10$  Å, these potential variations become negligible. Dashed lines indicate that close to the sample surface, the physics is not represented correctly due to finite electron density and the influence of ion cores.

by Ruffieux *et al.*<sup>5</sup> At that location, the LSP difference is about  $\Delta\phi = 2V_0 = 0.46$  eV (see Fig. 4), which is consistent with the measured shift of the first FER.

Experimentally observed LSP variations are now compared to DFT calculations. The resulting LSP, averaged in the direction parallel to the chains, is shown in Fig. 5. As indicated in Fig. 5, a maximum LSP difference of 0.3 eV is found at 3 Å above the surface defined by the plane of the Au ion cores. Thus the DFT calculation yields LSP differences quite comparable to those observed in the experiment.

Some examples of two-dimensional periodic modulations of the LSP observed via FER spectroscopy have been reported in the literature before, e.g., on a Ag/Pt(111) strain relief pattern<sup>5</sup> and on a NaCl/Ag(100) Moire pattern.<sup>39</sup> Compared to these examples, the one-dimensional modulation observed

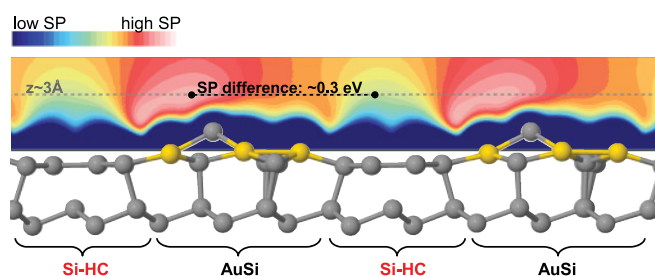


FIG. 5. (Color online) Theoretical electrostatic potential, obtained self-consistently from DFT calculations and averaged along the chain direction. A variant of the structural model in Fig. 1(b) was used in which the surface adatom density was set to the average experimental density of Fig. 1(a). A portion of the structural model is shown.

here is accompanied by significantly higher in-plane electric fields because the period length is much smaller (1.7 vs 7.8 nm<sup>39</sup> and  $\approx 7$  nm,<sup>5</sup> respectively) and the LSP variation is larger (0.46 vs 0.15 eV<sup>39</sup> and 0.35 eV,<sup>5</sup> respectively).

Perpendicular to the  $5 \times 2$  chains, the confined electron states of the FER cannot freely propagate because of the periodic LSP. This situation is similar to the herringbone reconstruction on Au(111), where the Shockley surface state is affected by the surface potential leading to a nonuniform local density of states (LDOS)<sup>40–42</sup> and the opening of minigaps at the surface Brillouin zone boundary (SBZB).<sup>43,44</sup> In the present STS data on  $5 \times 2$ , no indication for such an effect is observed. One reason is the relatively large distance between the tip and surface, suppressing contributions to the LDOS with large wave-vector components  $k_{\parallel}$  parallel to the surface. Furthermore, due to the low period length of less than 1.7 nm, contributions from the SBZB occur at much larger  $k_{\parallel}$  compared to the herringbone reconstruction on Au(111). Backfolding effects at the  $\bar{\Gamma}$  point are extremely small due to the low spectral weight, as verified by solving the central equation<sup>45</sup> for the  $5 \times 2$  potential.<sup>46</sup> Contributions of large  $k_{\parallel}$  (i.e., at voltages far above the FER onset) are also suppressed because of the influence of the feedback during closed-loop spectroscopy: the constant-current condition leads to tip retraction at the respective FER voltages, which in turn reduces the tunneling current and hence the  $dI/dV$  signal even if the LDOS remains constant as a function of voltage.

### C. Origin of fine structure on $5 \times 2$

The same mechanism based in the feedback-loop effect described above explains the origin of the double-peak feature of the first FER on the AuSi chains, which is absent on the Si-HC regions [cf. Fig. 3(c)]. A similar asymmetry effect has also been observed in an earlier publication on NaCl/Ag(100) without a detailed discussion.<sup>39</sup> The double peak originates from spectral overlap, i.e., partial contributions of both structures (the AuSi and SiHC chains) caused by the finite extent of the wave functions or the limited spatial resolution of the experiment [see Fig. 6(a)]. For an illustration, the  $dI/dV$  signal at constant current is simulated numerically based on a simple model LDOS consisting of broadened step functions, as shown in Fig. 6(b). Since the first FER is only weakly affected by the applied voltage, a free-electron-like dispersion is plausible, resulting in a stepped DOS. Within the Wentzel-Kramers-Brillouin (WKB) approximation, the tip displacement is numerically obtained from the tunneling expression:

$$I_T = \int_0^{eV} \rho_s \rho_t e^{-2\sqrt{\frac{2m\epsilon}{\hbar}} z \sqrt{\bar{\phi} + \frac{eV}{2} - E}} dE, \quad (2)$$

where  $\rho_s$  and  $\rho_t$  are the LDOS of the sample and tip, respectively, and  $\bar{\phi}$  is their mean work functions. The calculation of  $dI/dV$  at constant current results in the curves shown in Fig. 6(c) that can be compared qualitatively to the experiment in Fig. 3(c). The asymmetry with respect to the location (AuSi versus Si-HC) is clearly reproduced and most pronounced in the case of the AuSi chains. Even a small fraction from the Si-HC region results in a pronounced double-peak structure because the tip is still close to the sample at the energy onset

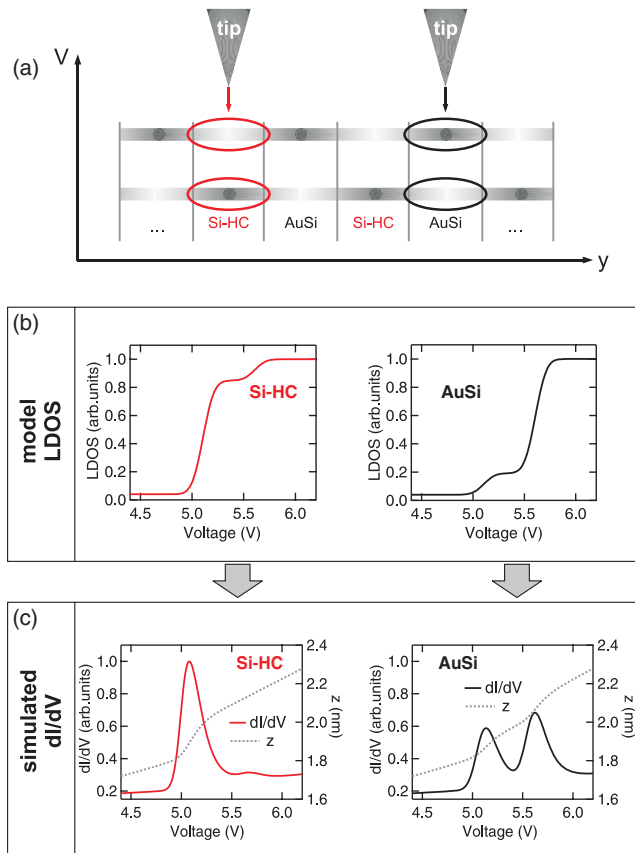


FIG. 6. (Color online) (a) Energy scheme of the first FER as a function of the lateral position perpendicular to the chains. Gray areas represent the probability density of the first FER eigenstates of the Si-HC (red line) and AuSi (black line) regions. (b) Corresponding model LDOS over Si-HC chains (red line) and over AuSi chains (black line) assuming a free-electron-like dispersion. (c) Simulated  $dI/dV$  signal (solid lines) and tip-sample distance  $z$  (dashed lines) according to the LDOS in (b). The small first step in the AuSi LDOS in (b) results in a pronounced signal in (c) due to the low tip-sample separation.

of the Si-HC FERs. In contrast, the second peak resulting from AuSi contributions is strongly suppressed on the Si-HC due to the large tip-sample separation at that energy. Hence,

a double-peak feature in the LDOS is much more prominent for a measurement over AuSi than over Si-HC, resulting in the observed splitting of the first FER peak in Fig. 3(c) and in the shoulder in the averaged spectrum in Fig. 2(c).

#### IV. SUMMARY

On patches of Si(111)-(7 × 7) and Si(111)-(5 × 2)-Au, the local work function has been compared using scanning tunneling spectroscopy of field-emission resonances. On both areas, the spectra differ mainly by a constant shift of 0.76 eV over the investigated energy range, directly reflecting the work-function difference. From the Fermi-level pinning reported in the literature, the contribution of surface dipoles is estimated to 0.27 eV. In addition, the local surface potential of Si(111)-(5 × 2)-Au has been mapped, yielding one-dimensional variations of 0.46 eV between the AuSi rows and the Si honeycomb chains at a distance of about 3 Å. All seven peak positions could be perfectly reproduced by a simple one-dimensional model taking into account the equilibration of the potential variations away from the surface. Local density calculations reproduce these modulations, albeit with smaller amplitude. Finally, the observed double-peak feature of the first FER on the AuSi chain is explained by a mechanism based on the lateral extension of FER states into neighboring chains in conjunction with the experimental boundary condition of a constant tunneling current during spectroscopy. In conclusion, a comprehensive and consistent picture of the surface potential on Si(111)-(5 × 2)-Au is established by combining the analysis of field-emission resonances with density-functional theory calculations. Pronounced surface-potential variations are found with large in-plane components of the electric field, which are of potentially significant impact on catalytic, electronic, and spin properties of nanostructured surfaces.

#### ACKNOWLEDGMENTS

We thank the Deutsche Forschungsgemeinschaft (DFG) for financial support within the SPP 1153. Part of this work was supported by the Office of Naval Research. The DFT computations were performed at the US DoD Major Shared Resource Centers at AFRL and ERDC. I.B. acknowledges stimulating discussions with Th. Fauster.

\*stefan.polei@uni-rostock.de

<sup>1</sup>I. Barke, F. Zheng, S. Bockenhauer, K. Sell, V. v. Oeynhausen, K. H. Meiwes-Broer, S. C. Erwin, and F. J. Himpsel, *Phys. Rev. B* **79**, 155301 (2009).

<sup>2</sup>S. C. Erwin, I. Barke, and F. J. Himpsel, *Phys. Rev. B* **80**, 155409 (2009).

<sup>3</sup>T. Okuda, K. Miyamaoto, Y. Takeichi, H. Miyahara, M. Ogawa, A. Harasawa, A. Kimura, I. Matsuda, A. Kakizaki, T. Shishidou, and T. Oguchi, *Phys. Rev. B* **82**, 161410 (2010).

<sup>4</sup>K. Wandelt, *Appl. Surf. Sci.* **111**, 1 (1997).

<sup>5</sup>P. Ruffieux, K. Aït-Mansour, A. Bendounan, R. Fasel, L. Patthey, P. Gröning, and O. Gröning, *Phys. Rev. Lett.* **102**, 086807 (2009).

<sup>6</sup>G. Binnig, K. H. Frank, H. Fuchs, N. Garcia, B. Reihl, H. Rohrer, F. Salvan, and A. R. Williams, *Phys. Rev. Lett.* **55**, 991 (1985).

<sup>7</sup>R. S. Becker, J. A. Golovchenko, and B. S. Swartzentruber, *Phys. Rev. Lett.* **55**, 987 (1985).

<sup>8</sup>K. H. Gundlach, *Solid-State Electron.* **9**, 949 (1966) [For an overview, see, e.g.,] P. D. Johnson and N. V. Smith, *Phys. Rev. B* **27**, 2527 (1983).

<sup>9</sup>D. Straub and F. J. Himpsel, *Phys. Rev. B* **33**, 2256 (1986).

<sup>10</sup>N. V. Smith, *Rep. Prog. Phys.* **51**, 1227 (1988).

<sup>11</sup>P. M. Platzman and M. I. Dykman, *Science* **284**, 1967 (1999).

<sup>12</sup>J. E. Ortega, F. J. Himpsel, R. Haight, and D. R. Peale, *Phys. Rev. B* **49**, 13859 (1994).

- <sup>13</sup>X. Y. Wang, X. J. Shen, R. M. Osgood, R. Haight, and F. J. Himpsel, *Phys. Rev. B* **53**, 15738 (1996).
- <sup>14</sup>M. Roth, T. Fauster, and M. Weinelt, *Appl. Phys. A* **88**, 497 (2007).
- <sup>15</sup>M. Roth, M. Pickel, W. Jinxiong, M. Weinelt, and T. Fauster, *Phys. Rev. Lett.* **88**, 096802 (2002); M. Roth, M. Pickel, J. Wang, M. Weinelt, and T. Fauster, *Appl. Phys. B* **74**, 661 (2002).
- <sup>16</sup>S. Smadici, D. Mocuta, and R. M. Osgood, *Phys. Rev. B* **69**, 035415 (2004).
- <sup>17</sup>T. K. Rügheimer, T. Fauster, and F. J. Himpsel, *Phys. Rev. B* **75**, 121401 (2007).
- <sup>18</sup>I. G. Hill and A. B. McLean, *Phys. Rev. Lett.* **82**, 2155 (1999).
- <sup>19</sup>J. A. Lipton-Duffin, J. M. MacLeod, and A. B. McLean, *Phys. Rev. B* **73**, 245418 (2006).
- <sup>20</sup>J. A. Lipton-Duffin, A. G. Mark, J. M. MacLeod, and A. B. McLean, *Phys. Rev. B* **77**, 125419 (2008).
- <sup>21</sup>H.-C. Ploigt, C. Brun, M. Pivetta, F. Patthey, and W.-D. Schneider, *Phys. Rev. B* **76**, 195404 (2007).
- <sup>22</sup>D. B. Dougherty, P. Maksymovych, J. Lee, M. Feng, H. Petek, and J. T. Yates, *Phys. Rev. B* **76**, 125428 (2007).
- <sup>23</sup>C. Schiller, A. A. Koomans, T. L. van Rooy, C. Schönenberger, and H. B. Elswijk, *Surf. Sci.* **339**, L925 (1995).
- <sup>24</sup>G. Kresse and J. Hafner, *Phys. Rev. B* **47**, 558 (1993).
- <sup>25</sup>G. Kresse and J. Furthmüller, *Phys. Rev. B* **54**, 11169 (1996).
- <sup>26</sup>T. Jung, Y. W. Mo, and F. J. Himpsel, *Phys. Rev. Lett.* **74**, 1641 (1995).
- <sup>27</sup>O. Y. Kolesnychenko, Y. A. Kolesnichenko, O. I. Shklyarevskii, and H. van Kempen, *Physica B* **291**, 246 (1999).
- <sup>28</sup>Note that tip geometry and tip-sample distance affect the parameter  $F$ , whereas the resulting  $\phi$  remains unchanged.
- <sup>29</sup>R. Losio, K. N. Altmann, and F. J. Himpsel, *Phys. Rev. B* **61**, 10845 (2000).
- <sup>30</sup>K. Sell, I. Barke, S. Polei, C. Schumann, V. von Oeynhausen, and K. H. Meiwes-Broer, *Phys. Status Solidi B* **247**, 1087 (2010).
- <sup>31</sup>F. Zheng, I. Barke, X. Liu, and F. J. Himpsel, *Nanotechnology* **19** (2008).
- <sup>32</sup>R. Bachmann, *Z. Phys.* **B8**, 31 (1968).
- <sup>33</sup>H. M. Zhang, T. Balasubramanian, and R. I. G. Uhrberg, *Phys. Rev. B* **65**, 035314 (2001).
- <sup>34</sup>S. Kitamura and M. Iwatsuki, *Appl. Phys. Lett.* **72**, 3154 (1998).
- <sup>35</sup>This follows from the fact that the wave function of the first FER is bound relatively close to the surface in the sample image potential, such that the additional electric field of the tunneling junction only has a little effect. See also Refs. 5 and 21.
- <sup>36</sup>J. Schnakenberg, *Algorithmen in der Quantentheorie und statistischen Physik* (Zimmermann-Neufang, Ulmen, 1995).
- <sup>37</sup>M. Kutschera, M. Weinelt, M. Rohlfing, and T. Fauster, *Appl. Phys. A* **88**, 519 (2007).
- <sup>38</sup>Within the simple one-dimensional model, a linear shape is assumed for the contact potential and the potential induced by the tip-sample voltage.
- <sup>39</sup>M. Pivetta, F. Patthey, M. Stengel, A. Baldereschi, and W.-D. Schneider, *Phys. Rev. B* **72**, 115404 (2005).
- <sup>40</sup>W. Chen, V. Madhavan, T. Jamneala, and M. F. Crommie, *Phys. Rev. Lett.* **80**, 1469 (1998).
- <sup>41</sup>L. Bürgi, H. Brune, and K. Kern, *Phys. Rev. Lett.* **89**, 176801 (2002).
- <sup>42</sup>T. Andreev, I. Barke, and H. Hövel, *Phys. Rev. B* **70**, 205426 (2004).
- <sup>43</sup>F. Reinert and G. Nicolay, *Appl. Phys. A* **78**, 817 (2004).
- <sup>44</sup>D. Malterre, B. Kierren, Y. Fagot-Revurat, S. Pons, A. Tejada, C. Didiot, H. Cercellier, and A. Bendounan, *New J. Phys.* **9**, 391 (2007).
- <sup>45</sup>C. Kittel, *Introduction to Solid State Physics* (Wiley, New York, 2005).
- <sup>46</sup>Similar results have been obtained for Au(111)<sup>44</sup> and vicinal metal surfaces.<sup>15</sup>